Eur. Phys. J. C 25, 405–411 (2002)
Digital Object Identifier (DOI) 10.1007/s10052-002-1023-x

THE EUROPEAN PHYSICAL JOURNAL C

Photoproduction of W bosons at HERA: QCD corrections*

K.-P.O. Diener[1], Ch. Schwanenberger[2,**], M. Spira[2]

[1] Institut für Theoretische Physik, Universität Karlsruhe, 76128 Karlsruhe, Germany
[2] Paul Scherrer Institut PSI, 5232 Villigen PSI, Switzerland

Received: 18 April 2002 /
Published online: 30 August 2002 – © Springer-Verlag / Società Italiana di Fisica 2002

Abstract. W bosons can be produced in the channels $e^{\pm}p \to W^{\pm} + X$ at HERA thus allowing to probe for anomalous trilinear couplings among the gauge bosons. We discuss the next-to-leading order (NLO) QCD corrections to the photoproduction of W bosons with finite transverse momentum at HERA. The higher-order QCD corrections reduce the factorization scale dependence significantly and modify the leading-order (LO) cross sections by $\pm\mathcal{O}(10\%)$.

1 Introduction

The study of W bosons at different colliders serves as an important test of the Standard Model and possible extensions. W bosons can be produced at the ep collider HERA with a center of mass (c.m.) energy $\sqrt{s} \approx 318$ GeV which is achieved by colliding electrons/positrons with energy $E_e = 27.5$ GeV and protons with energy $E_p = 920$ GeV. Since the production cross sections for the processes $e^{\pm}p \to e^{\pm}W + X$ reach values of about 1 pb at HERA, the production mechanisms of W bosons can be studied and the existence of anomalous $WW\gamma$ trilinear couplings can be probed [1–3]. Moreover, W boson production represents an important SM background to several new physics searches. In particular it is the dominant SM process leading to isolated high energy lepton events with missing transverse momentum [1,4]. In order to determine potential discrepancies between measurements and Standard Model (SM) predictions, the latter have to be sufficiently accurate and reliable. This is not guaranteed for the available LO calculations of W boson production [2,3,5]. For an unambiguous test of anomalous contributions, it is necessary to extend the previous analyses to NLO accuracy. The first step in this direction has been made in [6], where the QCD corrections to the total resolved photoproduction cross section have been determined. However, the result cannot be used for W boson production with large transverse momentum which is dominated by direct photoproduction, the QCD corrections to which are discussed in this letter.

* This work has been supported in part by the Swiss Bundesamt für Bildung und Wissenschaft, by the European Union under contract HPRN-CT-2000-00149 and by the DFG Research Group 'Quantenfeldtheorie, Computeralgebra und Monte-Carlo-Simulation'

** *Present address:* Deutsches Elektronen-Synchrotron DESY, 22603 Hamburg, Germany

2 Leading order

W boson production at ep colliders is mediated by photon, Z and W exchange between the electron/positron and the hadronic currents of the process. In general two phase-space regions are distinguished: the deep inelastic (DIS) regime at large Q^2 and the photoproduction regime at small Q^2, Q^2 being the negative square of the transferred momentum from the electron/positron. The photoproduction cross section can be calculated by convoluting the Weizsäcker-Williams photon spectrum,

$$f_{\gamma/e}(x_\gamma) = \frac{\alpha}{2\pi}\left\{\frac{1+(1-x_\gamma)^2}{x_\gamma}\log\frac{Q^2_{max}}{Q^2_{min}} - 2m_e^2 x_\gamma\left(\frac{1}{Q^2_{min}} - \frac{1}{Q^2_{max}}\right)\right\}, \quad (1)$$

with the differential hadronic cross section with respect to the transverse momentum p_{TW} and the rapidity y_W of the W boson for $\gamma q \to q'W$:

$$\frac{d^2\sigma^{dir}_{LO}}{dp_{TW}\,dy_W} = 2p_{TW}\sum_{q,\bar{q}}\int_{x_\gamma^-}^1 \frac{dx_\gamma}{x_\gamma} f_{\gamma/e}(x_\gamma) q_p(x_p,\mu_F^2) \times \frac{x_p}{s+u_1}\frac{s^2}{S}\frac{d\hat{\sigma}^{dir}_{LO}(\gamma q \to Wq')}{dt_1}, \quad (2)$$

where $q_p(x_p,\mu_F^2)$ is the corresponding quark density of the proton with momentum fraction x_p and at the factorization scale μ_F. $\hat{\sigma}^{dir}_{LO}(\gamma q \to Wq')$ denotes the corresponding LO partonic cross section and x_γ the photon momentum fraction of the electron/positron. (For the resolved part the Weizsäcker–Williams spectrum $f_{\gamma/e}$ has to be replaced by the convolution of $f_{\gamma/e}$ with the corresponding parton densities in the photon and the partonic cross section by the resolved expressions.) The QED coupling at

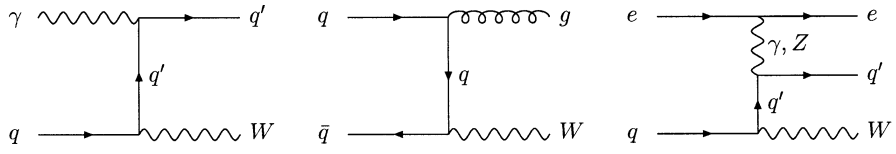

Fig. 1. Typical diagrams of W boson production with finite transverse momentum at HERA: direct, resolved and DIS mechanism

vanishing momentum transfer is denoted by α, the electron mass by m_e, and the minimal and maximal values of the photon virtuality Q^2 by Q^2_{min}, Q^2_{max}. In order to separate photoproduction from the DIS region we impose a cut of $Q^2_{max} = 4$ GeV^2 in the momentum transfer Q^2 from the electron/positron line. The minimal value of Q^2 is kinematically fixed,

$$Q^2_{min} = m_e^2 \frac{x_\gamma^2}{1 - x_\gamma}, \tag{3}$$

where negligible higher order terms in the electron mass m_e have been omitted. The partonic Mandelstam variables are defined as

$$\begin{aligned} s &= (k_1 + k_2)^2, \\ t &= (k_1 - p_1)^2, \qquad & t_1 &= t - M_W^2, \\ u &= (k_2 - p_1)^2, \qquad & u_1 &= u - M_W^2, \end{aligned} \tag{4}$$

where k_1 is the 4-momentum of the photon, k_2 the incoming quark 4-momentum and p_1 the 4-momentum of the outgoing W boson. The momentum fraction x_p of the proton is given by $x_p = x_p^-$, where

$$x_p^- = -\frac{x_\gamma T_1 + M_W^2}{x_\gamma S + U_1}, \tag{5}$$

and the lower bound of the x_γ integration by

$$x_\gamma^- = -\frac{U_1 + M_W^2}{S + T_1}. \tag{6}$$

S, T_1, U_1 denote the hadronic Mandelstam variables. They are related to the partonic variables as

$$s = x_\gamma x_p S, \qquad t_1 = x_\gamma T_1, \qquad u_1 = x_p U_1. \tag{7}$$

The hadronic Mandelstam variables can be expressed in terms of the transverse momentum p_{TW} and the rapidity y_W (defined to be positive in the electron/positron direction) of the W boson,

$$\begin{aligned} T_1 &= -\sqrt{S(p_{TW}^2 + M_W^2)}\, e^{-y_W - y_0}, \\ U_1 &= -\sqrt{S(p_{TW}^2 + M_W^2)}\, e^{y_W + y_0}, \end{aligned} \tag{8}$$

where $y_0 = \frac{1}{2} \log E_p/E_e$ denotes the shift in rapidity between the laboratory system and the hadronic c.m. system.

The leading direct photon process $\gamma q \to q' W$ (a typical contribution is depicted by the first diagram of Fig. 1) develops a singularity at LO when the final state quark q' becomes collinear with the initial state photon. However, the finite transverse momentum p_{TW} of the W boson has to be balanced by the final state quark, so that this singularity does not occur at LO for non-vanishing p_{TW}. The small Q^2 region includes the contribution of the hadronic component of the photon giving rise to $W + jet$ production via $q\bar{q}' \to Wg$ (second diagram of Fig. 1 as a typical example) and the crossed processes $gq(\bar{q}) \to Wq'(\bar{q}')$. The treatment of the DIS region is straightforward (a typical contribution is shown in the third diagram of Fig. 1).

The result for the direct contribution can be cast into the form

$$\begin{aligned} \frac{d\hat{\sigma}_{LO}^{dir}}{dt_1}[\gamma q \to Wq'] = &-\frac{G_F M_W^2 \alpha}{\sqrt{2}} \frac{(e_{q'} t_1 - e_W u)^2}{s^2 u t_1^2} \\ &\times \left(s^2 + u^2 + 2M_W^2 t\right), \end{aligned} \tag{9}$$

where G_F denotes the Fermi constant, M_W the W mass and $e_{q'}, e_W$ the electric charges of the scattered quark q' and W boson, i.e. $e_W = e_q - e_{q'} = \pm 1$. The LO cross sections of the resolved processes $q\bar{q}' \to Wg$ and $gq(\bar{q}) \to Wq(\bar{q})$ are given by ($C_F = 4/3$ and $T_R = 1/2$)

$$\begin{aligned} &\frac{d\hat{\sigma}_{LO}^{res}}{dt_1}[q\bar{q}' \to Wg] \\ &\quad = \frac{G_F M_W^2 \alpha_s}{3\sqrt{2}} C_F \frac{t^2 + u^2 + 2M_W^2 s}{s^2 t u}, \\ &\frac{d\hat{\sigma}_{LO}^{res}}{dt_1}[gq(\bar{q}) \to Wq'(\bar{q}')] \\ &\quad = -\frac{G_F M_W^2 \alpha_s}{3\sqrt{2}} T_R \frac{s^2 + u^2 + 2M_W^2 t}{s^3 u}, \end{aligned} \tag{10}$$

where α_s denotes the strong coupling constant.

The direct, resolved and DIS contributions add up to the total W p_{TW} distribution. Direct photoproduction develops the dominant contribution, while the DIS part is smaller but competitive. The resolved component is negligible for $p_{TW} \gtrsim 15$ GeV [7]. The consistency of the calculation requires that the dependence on the specific value of the cut Q^2_{max} which separates the DIS and photoproduction regimes, should be small. This dependence is presented in Fig. 2 for the LO W^+ and W^- cross sections at $p_{TW} = 40$ GeV. The residual dependence is below the per-cent level and thus indeed sufficiently small.

3 QCD corrections

For the dominant direct part we have evaluated the NLO QCD corrections. They consist of two parts, the virtual and real corrections. The virtual corrections are built up by all one-loop diagrams which are generated by virtual gluon exchange. Typical examples are displayed in Fig. 3.

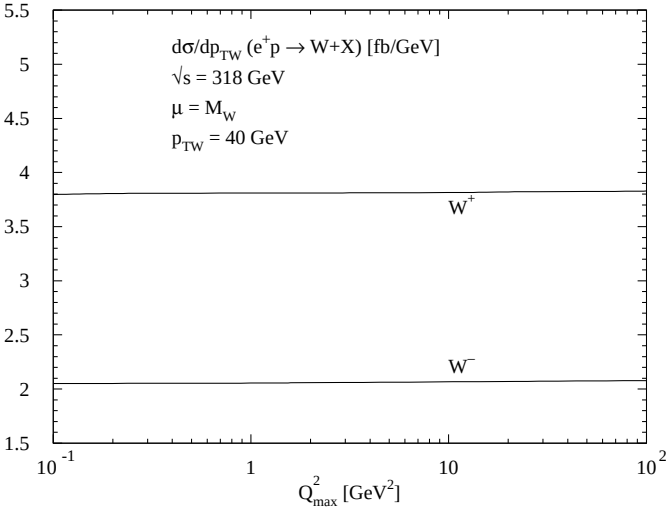

Fig. 2. Dependence of the differential LO $W^{\pm}$ production cross sections for $p_{TW} = 40$ GeV on the cut Q^2_{max} which separates the DIS and photoproduction regimes, after adding the DIS, direct and resolved contributions. The renormalization and factorization scales have been identified with the W mass, $\mu = \mu_F = \mu_R = M_W$

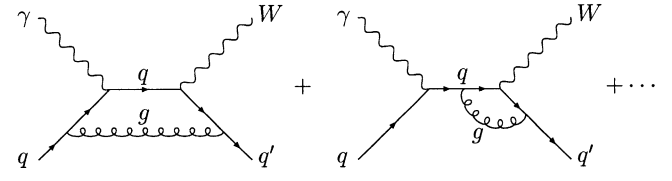

Fig. 3. Typical diagrams of the virtual corrections to direct photoproduction of W bosons at HERA

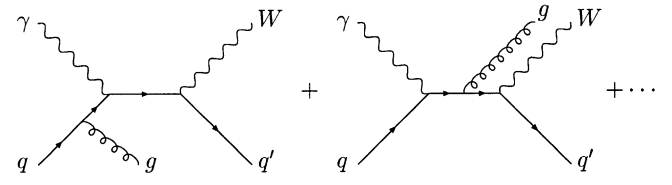

Fig. 4. Typical diagrams of the real corrections to direct photoproduction of W bosons at HERA

The real corrections originate from gluon radiation off the quark lines, see Fig. 4, and the corresponding crossed contributions with the gluon in the initial state.

The QCD-corrected result including virtual and real corrections can be cast into the form

$$\frac{d^2\sigma^{dir}_{NLO}}{dp_{TW}dy_W} = 2p_{TW}\sum_{h=q,\bar{q},g}\int_{x_\gamma^-}^1\frac{dx_\gamma}{x_\gamma}\int_{x_p^-}^1\frac{dx_p}{x_p} \times h_p(x_p,\mu_F^2)f_{\gamma/e}(x_\gamma)\frac{s^2}{S}\frac{d^2\hat{\sigma}^{dir}_{\gamma h}}{dt_1du_1} \quad (11)$$

with all parameters as defined in (4–8) and h_p denoting the corresponding parton density of the proton. The partonic virtual corrections are given by

$$\frac{d^2\hat{\sigma}_{virt}}{dt_1du_1} = \frac{d\hat{\sigma}_{virt}}{dt_1}\delta(s+t_1+u_1+M_W^2) \quad (12)$$

which leads to (2) with $\hat{\sigma}^{dir}_{LO}$ replaced by $\hat{\sigma}_{virt}$ for LO kinematics.

3.1 Virtual corrections

The virtual corrections have been computed via dimensional regularization in $n = 4-2\epsilon$ dimensions. The quarks have been treated as massless particles. Due to the Ward-Takahashi identities no renormalization is required after adding all diagrams, since there is no input parameter at LO which is affected by QCD corrections. The required scalar loop integrals are taken from [8]. The final double and single singularities of the virtual corrections arise from infrared gluon exchange and collinear singularities due to the gluon and massless quarks,

$$\frac{d\hat{\sigma}_{virt}}{dt_1} = C_{virt}C_F\frac{\alpha_s}{\pi}\frac{d\hat{\sigma}_{LO}}{dt_1}$$
$$C_{virt} = C_\epsilon\left\{-\frac{1}{\epsilon^2}-\frac{1}{\epsilon}\left(\frac{3}{2}+\log\frac{M_W^2}{-t}\right)+C_V\right\} \quad (13)$$

with

$$C_\epsilon = \Gamma(1+\epsilon)\left(\frac{4\pi\mu^2}{M_W^2}\right)^\epsilon \quad (14)$$

and a lengthy finite term C_V. These singularities are cancelled by adding the real corrections and the counter terms due to the renormalization of the parton densities.

As a cross check, the virtual corrections have also been evaluated by introducing small gluon and quark masses λ, m. This computation has been worked out with the programs FeynArts [9], FormCalc [10] and LoopTools [10]. The renormalization of the small quark mass has been performed in the $\overline{\rm MS}$ scheme to obtain an ultraviolet-finite result. The renormalization, however, does not affect the result in the limit of the massless gluons and massless quarks, but has to be introduced to take the massless limit in a consistent way. The infrared and collinear singularities now appear as logarithms of the gluon and quark masses in the limit of small masses,

$$C'_{virt} = C_\epsilon\left\{-\log\frac{\lambda^2}{-t}\log\frac{m^2}{-t}+\frac{1}{2}\log^2\frac{m^2}{-t} -\log\frac{\lambda^2}{-t}-\frac{1}{2}\log\frac{m^2}{-t}+C'_V\right\} \quad (15)$$

with a different finite term C'_V. This result has to be translated into the $\overline{\rm MS}$ scheme for zero masses. The corresponding piece to be added to the virtual corrections can be calculated from the results of [11,12] and it is given by

$$\Delta C_{virt} = C_\epsilon\left\{\log\frac{\lambda^2}{-t}\log\frac{m^2}{-t}-\frac{1}{2}\log^2\frac{m^2}{-t}+\log\frac{\lambda^2}{-t} +\frac{1}{2}\log\frac{m^2}{-t}-\frac{1}{\epsilon^2}-\frac{1}{\epsilon}\left(\frac{3}{2}+\log\frac{M_W^2}{-t}\right) -2-\frac{1}{2}\log^2\frac{M_W^2}{-t}-\frac{3}{2}\log\frac{M_W^2}{-t}\right\}. \quad (16)$$

After adding this transformation term to the virtual corrections C'_{virt} of the second approach, both results are in agreement.

3.2 Real corrections

The real corrections have been calculated by means of the massless dipole subtraction method introduced in [12]. The basic idea is to construct appropriate dipole terms $d\sigma^{sub}$ that include all infrared and collinear singularities of the real matrix elements, but can be integrated out analytically up to the LO phase space. The final expression for the differential cross section is given by

$$d\hat{\sigma}_{NLO} = d\hat{\sigma}_{LO} + [d\hat{\sigma}^{real} - d\hat{\sigma}^{sub}] + [d\hat{\sigma}^{virt} + d\bar{\hat{\sigma}}_1^{sub}] + [d\hat{\sigma}^{part} + d\bar{\hat{\sigma}}_2^{sub}], \quad (17)$$

where $d\bar{\hat{\sigma}}_{1,2}^{sub}$ are the two parts of the dipole terms which were integrated out analytically. They cancel the infrared and collinear divergences of the virtual corrections $d\hat{\sigma}^{virt}$ and the collinear singularity of the counter term $d\hat{\sigma}^{part}$ due to the renormalization of the parton densities at NLO, respectively. The NLO parton densities have been defined in the $\overline{\rm MS}$ scheme. Each of the square brackets in (17) is individually finite. This procedure allows to calculate the real matrix elements in 4 dimensions.

The dipole terms are constructed for each collinear and infrared configuration arising in the processes. They include the collinear singularities between final state partons themselves and those between the final state partons and the initial parton or photon. The collinear singularity related to the photon is absorbed by the renormalization of the direct part of the resolved photon densities. There is a subtlety in the numerical implementation of the dipole term corresponding to collinear $\gamma \to q\bar{q}$ splitting, see Fig. 5. Although this dipole term does not generate a new spurious singularity, the numerical integration turns out to be unstable, if the gluon in the final state is soft. In this case the quark emitted from the photon develops a large transverse momentum balancing the transverse momentum of the W boson. Since the dipole term has not been constructed to cover this case numerically, we introduced an upper cut on the product of photon and quark momenta,

$$2k_1p_2 < p_{cut}^2 \ . \quad (18)$$

After introducing this cut into the dipole terms which are subtracted from the real matrix element, and the analytically integrated one the numerical integration is stable and independent of this cut.

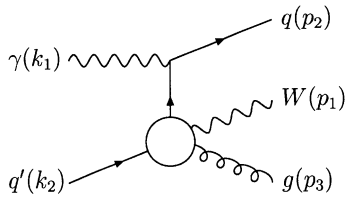

Fig. 5. Generic diagram developing the collinear singularity between the final state quark and the initial photon

4 Results

We analyze our final results for direct photoproduction of W bosons plus one jet $W+jet$ as well as the inclusive process $W+X$, i.e. without defining jets. We use the inclusive k_T algorithm for the jet definition with a cone size $R < 1$ [13]. Moreover, we require each detected parton in the final state to have transverse energy $E_T > 5$ GeV. One-jet configurations arise in this framework from 3 different phase space configurations: *(i)* LO kinematics include only one parton in the final state and are thus one-jet contributions automatically; *(ii)* if both partons of the real corrections are inside the same cone of size $R < 1$, they are combined to one jet; *(iii)* if one parton has $E_T < 5$ GeV, it is undetected so that only the other parton is counted as a single jet. The contributions of these three configurations have to be added to obtain the cross section for $W + 1$ jet production. The residual part of the real corrections is attributed to $W + 2$ jet production which has been added to the 1-jet part for the full $W + X$ production rate.

We have chosen CTEQ4M [14] and ACFGP [15] parton densities for the proton and the resolved photon, respectively. The strong coupling constant is taken at NLO with $\Lambda_5^{\overline{\rm MS}} = 202$ MeV. At LO we used CTEQ4L parton densities [14] with LO strong coupling and $\Lambda_5 = 181$ MeV. In our numerical analysis we have chosen the following values for the input parameters: $M_W = 80.43$ GeV, $M_Z = 91.1876$ GeV, $\alpha = 1/137.03599976$, $G_F = 1.16639 \times 10^{-5}$ GeV^{-2}, $m_e = 0.510998902$ MeV. In the fermionic Z couplings we have introduced the Weinberg angle $\sin^2\theta_W = 1 - M_W^2/M_Z^2$, and the Cabibbo angle between the first two generations has been chosen as $\sin\theta_c = 0.222$ [1].

Setting $\mu_R = \mu_F = M_W$ for the renormalization and factorization scales, we present the final results for the p_{TW} distributions of $W + 1$ jet and $W + X$ production in Fig. 6. The QCD corrections modify the direct contribution by about $\pm(10 - 15)\%$ and they are thus of moderate size. To estimate the theoretical uncertainties, the renormalization/factorization scale dependence of the direct contributions to the processes $e^+p \to W^\pm + X$ is presented in Fig. 7 for HERA conditions. The scale dependence is significantly smaller, once the NLO corrections are included. The residual scale dependence is reduced from about 20% down to about 5%. Figure 7 clearly indicates that the NLO QCD corrections are accidentially small at the central scale determined by the W boson mass. Since the uncertainties of the parton densities are of similar size, the total theoretical uncertainty can be estimated to be less than about 10%.

In Fig. 8 we present our final results for the total transverse momentum distributions of W^+ and W^- production at HERA including the NLO QCD corrections to the direct photoproduction part. The individual contributions are also shown. The Figure clearly demonstrates the dominance of the direct photoproduction part, while the DIS part is smaller but still relevant. The resolved photopro-

[1] In our numerical analysis we neglected the contribution of initial b quarks

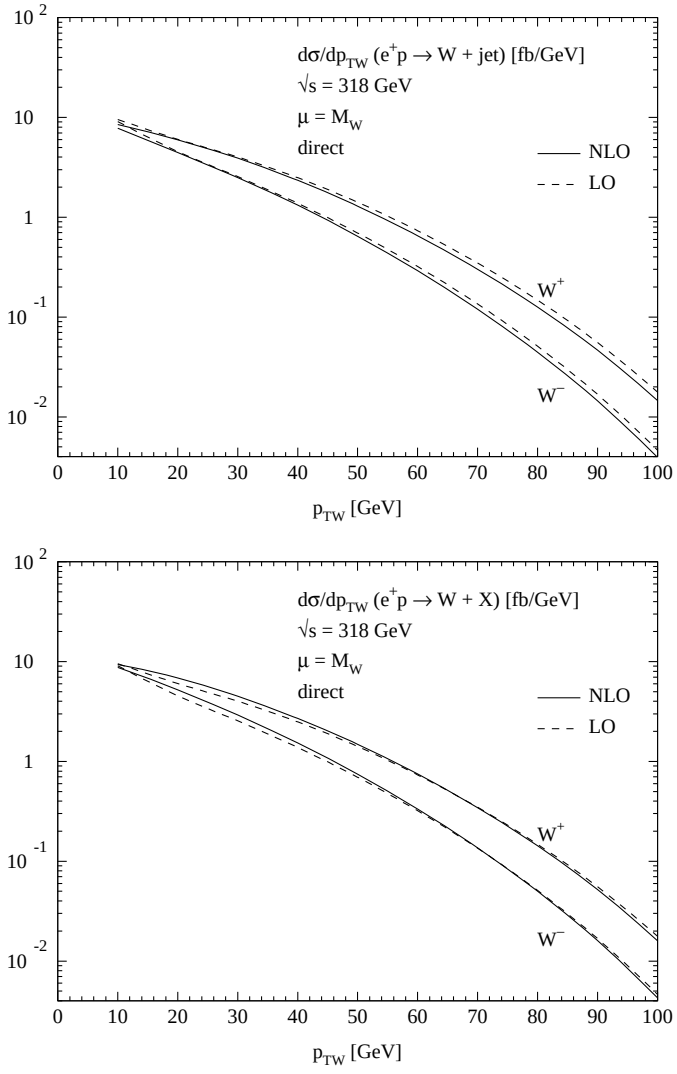

Fig. 6. Transverse momentum distribution of W bosons at HERA for direct photoproduction. The full curves show the NLO p_{TW} distributions, while the broken lines exhibit the LO distributions. The upper plot shows $W + 1jet$ production and the lower the total sum of $W + X$ production

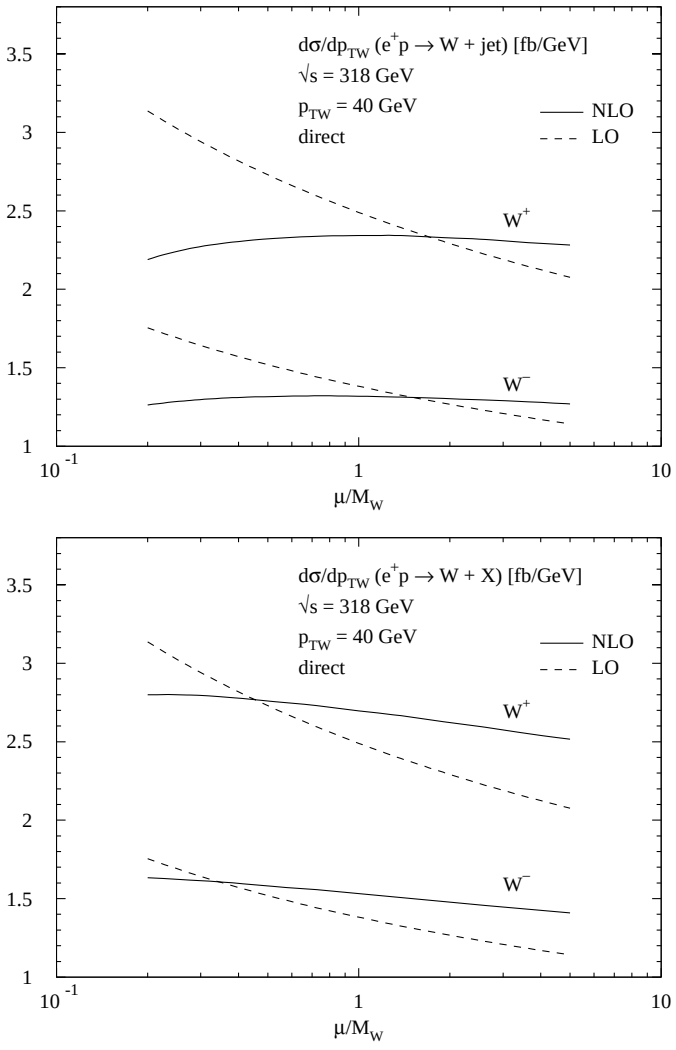

Fig. 7. Dependence of the direct contribution to W production on the renormalization and factorization scale $\mu = \mu_F = \mu_R = \xi M_W$ for $p_{TW} = 40$ GeV. The full curves represent the NLO predictions and the broken curves the LO scale dependences. The upper plot presents $W + 1jet$ production and the lower the total sum of $W + X$ production

duction part can safely be neglected for p_{TW} values larger than about $10 - 15$ GeV. The rising total sum at p_{TW} values below about 15 GeV signals the breakdown of the pure perturbative results and underlines the necessity of a soft gluon resummation to describe W boson production for smaller transverse momenta which however is beyond the scope of this work.

The rapidity distribution of W boson production at HERA for $p_{TW} = 40$ GeV is presented in Fig. 9 for all individual parts. The direct photoproduction part is shown at LO and NLO. As in the case of the transverse momentum distribution the QCD corrections to the direct contribution amount to less than about $10 - 15\%$ and are of moderate size. They hardly change the shape of the rapidity distribution. It can clearly be inferred from this figure that there is a preference to produce W bosons at larger values of the rapidity y_W.

In order to allow a comparison of our results with existing analyses at HERA, we have determined the cross sections for transverse momenta below and above 25 GeV. In the first case we have used the NLO results of [6,7] for the cross section with $p_{TW} < 25$ GeV, while for $p_{TW} > 25$ GeV we have integrated our results including the NLO corrections to direct photoproduction. We obtain the following values for the cross section in the case of a positron beam (the numbers in brackets are the LO values):

$$\begin{aligned} p_{TW} < 25 \text{ GeV} : \sigma(W^+) &= 0.478 \text{ pb} \quad (0.363 \text{ pb}) \\ \sigma(W^-) &= 0.484 \text{ pb} \quad (0.348 \text{ pb}) \\ p_{TW} > 25 \text{ GeV} : \sigma(W^+) &= 0.150 \text{ pb} \quad (0.143 \text{ pb}) \\ \sigma(W^-) &= 0.084 \text{ pb} \quad (0.079 \text{ pb}) \, . \end{aligned} \tag{19}$$

No other cuts have been imposed.

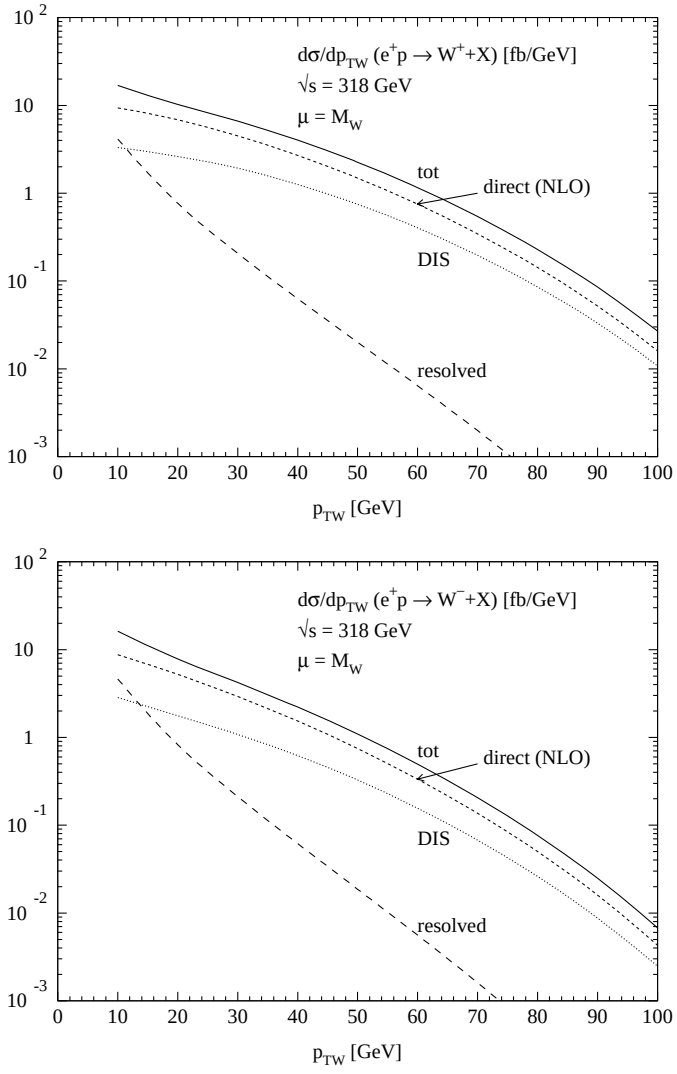

Fig. 8. Transverse momentum distributions of W bosons at HERA. The full curves show the total p_{TW} distributions, while the broken lines exhibit the individual LO DIS, NLO direct and LO resolved contributions. The upper plot is for W^+ production and the lower for W^- bosons

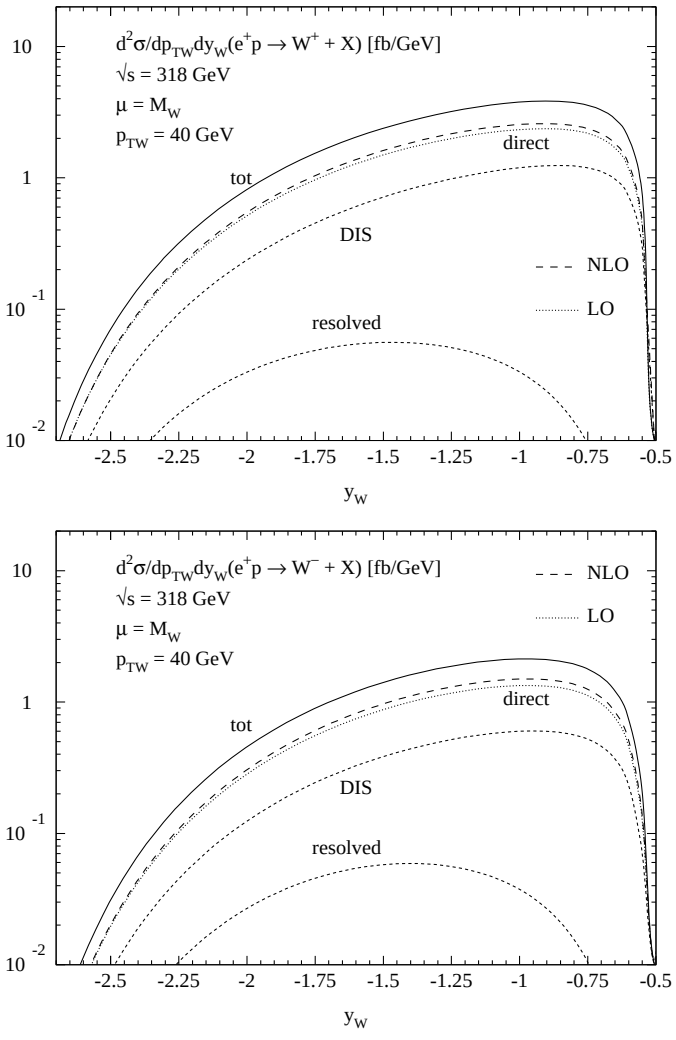

Fig. 9. Rapidity distribution of W bosons at HERA at $p_{TW} = 40$ GeV. The full curves show the total distributions including the NLO corrections to the direct contribution, while the broken lines exhibit the individual parts at LO and the direct part at NLO. The upper plot presents W^+ production and the lower plot W^- production

5 Conclusions

We have presented predictions for W boson production at HERA including the QCD corrections to the dominant direct photon mechanism at finite transverse momentum of the W bosons. Working in the conventional $\overline{\rm MS}$ scheme we find that the QCD corrections modify the direct contribution by about $\pm(10-15)\%$ at the nominal renormalization/factorization scale $\mu_R = \mu_F = M_W$ and are thus of moderate size. In addition, the NLO corrections reduce the residual scale dependence of direct photoproduction to a level of about 5%. Taking into account also the uncertainties in the parton densities of the proton and the photon, the total theoretical uncertainty is estimated to be about 10%. However, the QCD corrections to the DIS part are still unknown. They are not expected to be significantly larger, because they have to cancel the Q^2_{max} dependence of the NLO direct contribution and thus have to be of similar size. Since the QCD corrections are dominated by soft gluon effects, the shapes of the differential distributions are hardly affected. Therefore the results obtained in this work cannot explain the excess of isolated high-energy lepton events observed at the H1 experiment [4].

Acknowledgements. We would like to thank S. Catani, C. Diaconu, R. Eichler, E. Elsen, M. Kuze, A. Mehta, P. Schleper and P.M. Zerwas for useful discussions. We are grateful to C. Diaconu, P. Schleper and P.M. Zerwas for carefully reading the manuscript.

References

1. J. Breitweg et al., ZEUS Collaboration, Phys. Lett. B **471**, 411 (2000)

2. U. Baur, J.A.M. Vermaseren and D. Zeppenfeld, Nucl. Phys. B **375**, 3 (1992)
3. M.N. Dubinin and H.S. Song, Phys. Rev. D **57**, 2927 (1998)
4. C. Adloff et al., H1 Collaboration, Eur. Phys. J. C **5**, 575 (1998); H1 Collaboration, Proceedings EPS2001, contributed paper 802, Budapest, 2001
5. C.H. Llewellyn-Smith and B.H. Wiik, Report DESY 77/38; P. Salati and J.C. Wallet, Z. Phys. C **16**, 155 (1982); K. Neufeld, Z. Phys. C **17**, 145 (1983); A.N. Kamal, J.N. Ng and H.C. Lee, Phys. Rev. D **24**, 2842 (1984); G. Altarelli, G. Martinelli, B. Mele and R. Rückl, Nucl. Phys. B **262**, 204 (1985); E. Gabrielli, Mod. Phys. Lett. A **1**, 465 (1986); M. Böhm and A. Rosado, Z. Phys. C **34**, 117 (1987) and Z Phys. C **39**, 275 (1988); U. Baur and D. Zeppenfeld, Nucl. Phys. B **325**, 253 (1989); J. Blümlein and G.A. Schuler, preprint PHE-90-21, in proceedings "Snowmass 1990, Research directions for the decade"; M. Janssen, Z. Phys. C **52**, 165 (1991); C.S. Kim and W.J. Stirling, Z. Phys. C **53**, 601 (1992)
6. P. Nason, R. Rückl and M. Spira, Proceedings of the 3rd UK Phenomenology Workshop on HERA Physics, Durham, 1998, J. Phys. G **25**, 1434 (1999)
7. M. Spira, Proceedings "Workshop on Monte Carlo Generators for HERA Physics", Hamburg, 1998, hep-ph/9905469
8. K. Fabricius and I. Schmitt, Z. Phys. C **3**, 51 (1979); R.K. Ellis, D.A. Ross and A.E. Terrano, Nucl. Phys. B **178**, 421 (1981)
9. J. Küblbeck, M. Böhm and A. Denner, Comput. Phys. Commun. **60**, 165 (1990); H. Eck and J. Küblbeck, *Guide to FeynArts 1.0*, Univ. Würzburg, 1992
10. T. Hahn and M. Perez-Victoria, Comp. Phys. Comm. **118**, 153 (1999)
11. B. Humpert and W.L. van Neerven, Nucl. Phys. B **194**, 225 (1981); S. Dittmaier, Nucl. Phys. B **565**, 69 (2000)
12. S. Catani and M.H. Seymour, Nucl. Phys. B **485**, 291 (1997), (E) *ibid* B **510**, 503 (1997)
13. S. Catani, Y.L. Dokshitzer, M.H. Seymour and B.R. Webber, Nucl. Phys. B **406**, 187 (1993); S.D. Ellis and D.E. Soper, Phys. Rev. D **48**, 3160 (1993)
14. H.L. Lai, J. Huston, S. Kuhlmann, F. Olness, J. Owens, D. Soper, W.K. Tung and H. Weerts, Phys. Rev. D **55**, 1280 (1997)
15. P. Aurenche, P. Chiappetta, M. Fontannaz, J.P. Guillet and E. Pilon, Z. Phys. C **56**, 589 (1992)